Frontiers in Bioscience Landmark

Front. Biosci. (Landmark Ed) **2026**; 31(9): 53367
https://doi.org/10.31083/FBL53367

Original Research

PIAS2 Overexpression Attenuates Erastin-Induced Ferroptotic Changes and Is Associated With Increased GPX4 Protein and Enhanced GPX4-Related SUMO3 Signaling in Hepatocellular Carcinoma Cells

Xiang Cai[1], Jiangwei Ye[1], Linfu Fang[1], Xiaokun Ding[1], Zejun Fang[2], Ming Ye[1,*]

[1]Department of General Surgery, Sanmen People's Hospital, 317100 Sanmen, Zhejiang, China
[2]Central Laboratory, Sanmen People's Hospital, 317100 Sanmen, Zhejiang, China
*Correspondence: yeming@zjsmyy.com (Ming Ye)
Academic Editor: Sung Eun Kim
Submitted: 28 April 2026 Revised: 29 June 2026 Accepted: 23 July 2026 Published: 7 September 2026

Abstract

Background: Protein inhibitor of activated STAT 2 (PIAS2) is highly expressed in various solid tumors. Its precise function as a ferroptosis regulator in hepatocellular carcinoma (HCC) is still unknown. The purpose of this work was to determine whether PIAS2 overexpression attenuates erastin-induced ferroptotic changes and, in turn, is associated with the development of HCC in a manner that correlates with changes in Glutathione Peroxidase 4 (GPX4) protein levels and small ubiquitin-like modifier 3 (SUMO3) modification signals. **Methods:** Erastin (Era) was used to induce ferroptosis in HepG-2 and H22 cells, while Ferrostatin-1 (Fer-1) was employed for validation. Western blotting, qPCR, and co-immunoprecipitation (Co-IP) were used to examine the expression and interaction of PIAS2 and GPX4. Ferroptosis markers (lipid-reactive oxygen species (ROS), malondialdehyde (MDA), glutathione (GSH), Fe^{2+}), cell viability, migration, and invasion were all analyzed. Functional rescue experiments were performed using PIAS2 overexpression (oe-PIAS2) and GPX4 knockdown (sh-GPX4). In addition, a murine model of H22 cells in the right groin/lateral abdomen was established for *in vivo* validation. Tumor weight and volume were measured in these animals. Additionally, tumor tissues were collected and subjected to immunohistochemical staining for Ki-67 expression, as well as biochemical analysis of ferroptosis-related markers (GSH, MDA, Fe^{2+}). **Results:** In HCC cells, Era-induced ferroptosis resulted in a significant downregulation of PIAS2 and GPX4 expression, as well as elevated levels of lipid ROS, MDA, and Fe^{2+}, decreased GSH content, and decreased cell viability, migration, and invasion. Under Era-treated conditions, overexpression of PIAS2 effectively reversed these changes, suppressing ferroptosis and partially restoring malignant phenotypes within the context of Era challenge. Co-treatment with Fer-1 significantly reversed Era-induced ferroptotic changes and rescued cell viability, migration, and invasion, without affecting PIAS2 expression, while also restoring GPX4 levels. Mechanistic studies revealed that PIAS2 and GPX4 co-immunoprecipitate in HCC cells, and PIAS2 overexpression was associated with increased SUMO3 modification signals and higher remaining GPX4 protein levels at the examined 12- and 24-h CHX time points. GPX4 knockdown attenuated the phenotypes observed under PIAS2 overexpression, suggesting possible involvement of GPX4 in the effects of PIAS2. In Era-treated tumor-bearing mice, PIAS2 overexpression was associated with increased tumor growth, elevated Ki-67 and GPX4 levels, and reduced ferroptosis indicators. **Conclusion:** PIAS2 overexpression was associated with increased GPX4 SUMO3 modification signals and higher GPX4 protein levels at the examined CHX time points, together with reduced ferroptotic changes under Era-treated conditions.

Keywords: carcinoma; ferroptosis; phospholipid hydroperoxide glutathione peroxidase; SUMO-3 protein; tumor burden; hepatocellular

1. Introduction

One of the most prevalent cancers in the world, hepatocellular carcinoma (HCC) poses a serious risk to human health due to its continuously growing incidence and ranking as the third most common cause of cancer-related death [1]. Owing to the liver's strong compensatory capacity, early-stage HCC is often asymptomatic, such that in most cases it is only diagnosed in a more advanced stage, at which time patients have missed the optimal window for curative resection. The overall prognosis for HCC patients is still dismal, with a low five-year survival rate, despite recent advancements in the development of more effective targeted treatments and immunotherapies [2]. In order to improve clinical outcomes, it is crucial to understand the molecular mechanisms underlying the development of HCC and to find new treatment targets.

Ferroptosis is an iron-dependent kind of cell death that differs from autophagy, necrosis, and apoptosis in terms of its genetic regulation, biochemical dynamics, and morphological presentation. Its defining characteristic is the iron-dependent build-up of lipid hydroperoxides, and one important biological characteristic is a substantial rise in intracellular ferrous ions. Excess ferrous ions can cause ferroptosis by catalyzing the production of reactive oxygen

species (ROS) and starting a cascade of lipid peroxidation [3]. Ferroptosis plays a critical role in the formation and evolution of a variety of malignancies, and its dysregulation is strongly linked to malignant characteristics such as invasion, metastasis, and treatment resistance, according to an increasing amount of data [4,5,6]. Research has demonstrated that ferroptosis induction significantly suppresses tumor development in HCC, whereas ferroptosis inhibition enhances HCC advancement [7,8]. According to these results, treating HCC may benefit from focusing on the ferroptosis pathway.

Small ubiquitin-like modifier (SUMO) modification is one type of post-translational modification capable of regulating a range of cellular processes by influencing target protein stability, nucleocytoplasmic transport, protein-protein interactions, and transcriptional activity [9]. There is strong evidence for the aberrant regulation of SUMOylation in HCC, where it contributes to tumor progression by affecting HCC cell proliferation, apoptosis, invasion, and metastasis [10]. Tumor tissues have been shown to produce more protein inhibitor of activated STAT 2 (PIAS2), a member of the PIAS family of SUMO E3 ligases, than nearby normal tissues [11]. Nevertheless, the exact molecular processes by which PIAS2 controls the development of HCC are still unclear, and its possible role in controlling ferroptosis has not yet been fully explored.

A critical component of the glutathione system, glutathione peroxidase 4 (GPX4) is essential for maintaining intracellular redox equilibrium. GPX4 primarily converts lipid hydroperoxides into non-toxic lipid alcohols, shielding cells from damage caused by oxidative stress [12]. GPX4 is a crucial ferroptosis negative regulator that is closely linked to the ferroptosis pathway in a number of malignancies [13,14]. Furthermore, there is strong evidence that GPX4 can be SUMOylated, thereby regulating ferroptotic activity [15]. For instance, by controlling GPX4 SUMOylation, bone marrow stromal cells can prevent ferroptosis in myeloma cells [16]. However, whether PIAS2, as a SUMO E3 ligase, can modulate GPX4 SUMOylation and thereby be associated with ferroptosis and progression in HCC cells has not been reported. Therefore, the current study's goal was to use complementary *in vitro* and *in vivo* methods to examine the association between PIAS2's modulatory effects on GPX4 SUMOylation and ferroptosis in HCC cells, providing fresh functional insight into a novel therapeutic target in this fatal cancer type.

2. Materials and Methods

2.1 Grouping and Cell Culture

Wuhan Procell Life Technology Co., Ltd. supplied the H22 cells (CL0341) and HepG-2 cells (CL-0103). The cells were grown at 37 °C in a humidified incubator with 5% CO_2 in DMEM (Gibco, Waltham, MA, USA, 11965092) supplemented with 10% fetal bovine serum (FBS, Gibco, 10099141C) and 1% penicillin/streptomycin (Gibco, 15140122). All cell lines were negative for mycoplasma contamination and were verified using STR profiling. The following groups of cells were created: Control (Con), Erastin (Era), Era+oe-NC, Era+oe-PIAS2, and Era+Fer-1 groups. The Con group underwent standard culture. The Era group was treated with 10 μM Era (MedChemExpress, Monmouth Junction, NJ, USA, HY-15763) for 24 hours [17]. For the Era+oe-NC and Era+oe-PIAS2 groups, cells were first transfected with the indicated constructs (oe-NC or oe-PIAS2) for 48 hours, followed by treatment with 10 μM Erastin for an additional 24 hours. The Era+Fer-1 group was co-treated with 10 μM Era and 10 μM Ferrostatin-1 (Fer-1, MedChemExpress, HY-100579) for 24 hours. For all groups, final analyses were performed at the end of the 24-hour drug treatment period (i.e., 72 hours after the start of transfection for transfected groups).

2.2 Cell Transfection

Following an overnight culture, transfection was carried out in accordance with the manufacturer's instructions using Lipofectamine 3000 (Thermo Fisher Scientific, Waltham, MA, USA, L3000015). As needed, oe-PIAS2, oe-NC, sh-GPX4, sh-PIAS2 or sh-NC constructs were transfected into cells at a final concentration of 50 nM for shRNA constructs and 2 μg/mL for overexpression plasmids. Four hours after transfection, the media was changed, and the cells were then grown for a further 48 hours. Shanghai GenePharma Co., Ltd. (Shanghai, China) created all of the vectors. The following sequences were used for construct generation: sh-PIAS2: 5′-GCAAGAGTTGCTACAGCATTT-3′; sh-GPX4: 5′-GCTCATCACCGGTTCCCATTA-3′; sh-NC: 5′-TTCTCCGAACGTGTCACGT-3′.

2.3 Animal Model and Treatment

Hunan Silaike Jingda Experimental Animal Co., Ltd. (Changsha, Hunan, China) supplied twenty-four male BALB/c nude mice that were between four and six weeks old. Mice were kept in a particular pathogen-free habitat with a temperature of 22 ± 1 °C, a relative humidity of 50–60%, a 12-hour light/dark cycle, and full access to food and drink. H22 cells in the logarithmic growth phase were resuspended in PBS and adjusted to a density of 1×10^7 cells/mL following a week of acclimatization. Each mouse's right flank received a subcutaneous injection of a 200 μL cell solution. Seven days after inoculation, when visible tumors had developed (mean tumor volume ± SD: 98.3 ± 15.6 mm^3), mice were randomized into four groups (Con, Era, Era+oe-NC, and Era+oe-PIAS2) by a researcher blinded to treatment using a computer-generated random number sequence. Baseline tumor volumes showed no significant difference among groups ($p > 0.05$). For two weeks, mice in the Era, Era+oe-NC, and Era+oe-PIAS2 groups were given intraperitoneal injections of Era (20 mg/kg) every other day in a vehicle con-

sisting of 5% DMSO + 40% PEG300 + 5% Tween 80 + 50% saline (prepared fresh before each injection) [18]. An equivalent amount of vehicle (5% DMSO + 40% PEG300 + 5% Tween 80 + 50% saline) was given to the Con group. Adeno-Associated Virus (AAV) vectors were constructed using AAV8 serotype with a CMV/CBA hybrid promoter driving the PIAS2 coding sequence or empty vector (oe-NC). The viral titer was 1×10^{12} vg/mL, and each mouse received 1×10^{11} vg (100 µL) via tail vein injection. Based on preliminary validation experiments in our laboratory, PIAS2 protein expression begins to rise approximately 24–48 hours after AAV injection and remains elevated throughout the experimental period. AAV vectors were administered 30 minutes before the first Era injection. This timing was chosen to minimize the interval between AAV delivery and erastin administration to ensure that the overexpression vector is present systemically prior to ferroptosis induction. The effects observed reflect sustained overexpression following AAV transduction over the two-week treatment period, with erastin administration starting immediately after AAV delivery to maintain temporal alignment across all experimental groups. Mice were given an intraperitoneal injection of 1% sodium pentobarbital (Sigma, Burlington, MA, USA, P3761, 50 mg/kg) to induce anesthesia twenty-four hours following the last treatment, and they were terminated by cervical dislocation. Calipers were used to measure, weigh, and remove the tumors. The tumor volume (mm^3) was computed as (length × $width^2$)/2. Tumors were imaged and kept at –80 °C. The complete experimental timeline was as follows: Day 0, H22 cell inoculation; Day 7, visible tumor formation and randomization into groups; Day 7, AAV injection (30 min before first Era dose); Days 7–20, Era injection every other day (total of 7 injections); Day 20, tumor collection and analysis. Animal study was approved by the Institutional Animal Care and Use Committee of Zhejiang Provincial Laboratory Animal Center (Approval No.: ZJCLA-IACUC-20011376).

2.4 CCK-8 Cell Viability Assay

After being seeded at a density of 8×10^3 cells per well in 96-well plates, the cells were cultivated for a full day. Following the treatment protocol described in Section 2.1 (48-hours transfection followed by 24-hours drug treatment), Cell Counting Kit-8 (CCK-8) reagent (MedChemExpress, Monmouth Junction, NJ, USA, HY-K0301) was added at the end of the 24-hour drug treatment period. This was followed by a 1.5-hour dark incubation period. A microplate reader was used to measure absorbance at 450 nm. The formula for calculating cell viability was: (Absorbance of the experimental group–Absorbance of the blank group)/(Absorbance of the control group – Absorbance of the blank group) × 100%. The complete timeline for CCK-8 experiments was: Day 0, cell seeding; Day 1, transfection (for transfected groups) or no treatment (for Control and Era groups); Day 3 (48 h post-transfection), Erastin treatment (for drug-treated groups) for 24 hours; Day 4, CCK-8 reagent addition and measurement.

2.5 Measurement of Cellular Lipid ROS Levels

HepG-2 and H22 cells were seeded in 6-well plates and treated according to the protocol described in Section 2.1 (48 h transfection followed by 24 h drug treatment). At the end of the drug treatment period, cells were stained and analyzed. After staining the cells with 10 µmol/L BODIPY 581/591 C11 (Thermo Fisher Scientific, D3861) in DMEM, the cells were incubated for 30 minutes at 37 °C. Cells were examined under an inverted fluorescent microscope following two PBS washes. ImageJ (Bethesda, MD, USA) was used to measure the relative fluorescence intensity of lipid ROS. The timeline was: Day 0, cell seeding; Day 1, transfection (for transfected groups) or no treatment (for Control and Era groups); Day 3 (48 h post-transfection), Erastin treatment (for drug-treated groups) for 24 hours; Day 4, staining and imaging.

2.6 Determination of GSH, MDA, and Fe^{2+} Content

Treated cells were collected at the end of the 24-hour drug treatment period (i.e., 72 hours after transfection initiation for transfected groups) for biochemical analysis. Approximately 10 mg of tumor tissue was collected, lysed or homogenized, and centrifuged to obtain supernatant for analysis. Malondialdehyde (MDA) and glutathione (GSH) levels were measured using thiobarbituric acid colorimetry and DTNB colorimetric methods (Nanjing Jiancheng Bioengineering Institute, Nanjing, Jiangsu, China; MDA: A003-1-2, GSH: A006-2-1). The Ferrous Iron Colorimetric Assay Kit (Elabscience, Wuhan, Hubei, China, E-BC-K773-M) was used to measure absorbance at 593 nm and calculate Fe^{2+} concentration in accordance with the kit's instructions. All biochemical parameters (GSH, MDA, Fe^{2+}) were normalized to total protein concentration in the same samples, which was determined using a BCA protein assay kit (Beyotime, Shanghai, China, P0010). Results are expressed as µmol/g protein.

2.7 Western Blotting

Proteins were extracted from cells at the end of the 24-hour drug treatment period (72 hours after transfection initiation for transfected groups) or from tumor tissues. SDS-PAGE was used to separate the proteins, which were then deposited onto PVDF membranes (Millipore, Burlington, MA, USA, BM3PB0236A) at 100 V in an ice bath. After blocking the membranes with 5% non-fat milk for two hours, the membranes were incubated with primary antibodies at 4 °C for sixteen to twenty hours while being gently shaken. Following TBST washing, membranes were incubated for 90 minutes at room temperature with matching HRP-conjugated secondary antibodies (Biosharp, Beijing, China, BL003A). Following washing, proteins were scanned using a Tanon-5200 chemiluminescence imaging

system (Shanghai Tanon Technology Co., Ltd., Shanghai, China) and observed using ECL chemiluminescent substrate (BIOMIKY, Shanghai, China, MK042A). ImageJ was used to assess band intensity. Primary antibodies used for this experiment included those specific for the following: PIAS2 (Abcam, Cambridge, UK, ab137825, 1:1000), GPX4 (Abcam, ab125066, 1:2000), β-actin (Cell Signaling Technology, Danvers, MA, USA, 4970, 1:5000).

2.8 Co-Immunoprecipitation (Co-IP) and SUMOylation Level Detection

Total protein was obtained by collecting and lysing HepG-2 and H22 cells after 48 hours of transfection. After adding pre-equilibrated protein A/G magnetic beads (Santa Cruz Biotechnology, Dallas, TX, USA, sc-2003), the mixture was incubated for a further four hours. Centrifugation was used to collect and wash the beads. To assess protein-protein association, the immunoprecipitated complexes were subjected to Western blotting using anti-GPX4 and anti-PIAS2 antibodies.

For detection of GPX4 SUMOylation, cells were transfected with Flag-GPX4 constructs along with oe-PIAS2, sh-PIAS2, or corresponding controls for 48 hours. Cell lysates were first denatured by boiling in 1% SDS for 10 minutes to break non-covalent contacts before being diluted ten times with lysis buffer to lower the SDS content. Anti-Flag (Sigma-Aldrich, F1804, 1:100) was used to immunoprecipitate Flag-GPX4 from the denatured lysates overnight at 4 °C. After adding protein A/G magnetic beads, the mixture was incubated for a further four hours. After extensive washing, the immunoprecipitated complexes were eluted and analyzed by Western blotting using anti-SUMO3 (Abcam, ab217862, 1:1000). Input controls were also probed for Flag, GPX4 and SUMO3 to confirm equal protein loading and successful immunoprecipitation. SUMOylation levels are presented as representative blots and described qualitatively.

2.9 Transwell Invasion Assay and Migration Assay

For the invasion assay, 50 µL of Matrigel (Corning, Corning, NY, USA, 356234) was applied to transwell chambers that included membranes with an 8 µm pore size (Corning) in 24-well plates. Following treatment according to the protocol described in Section 2.1 (48 h transfection followed by 24 h drug treatment), cells were harvested at the end of the 24-hour drug treatment period and resuspended at 1×10^5 cells/mL in serum-free DMEM. Next, 600 µL of DMEM media with 10% FBS was added to the lower chamber and 200 µL of cell suspension was added to the top chamber. Non-invading cells on the top surface were eliminated during a 48-hour incubation period. After invading cells were fixed for 15 minutes with 4% paraformaldehyde (Servicebio, Wuhan, Hubei, China, G1101), they were stained for 10 minutes with 0.1% crystal violet (Sigma, C0775). Invaded cells were examined and tallied under a microscope following washing.

For the migration assay (performed in parallel without Matrigel), the same procedure was followed except that the transwell membrane was not coated with Matrigel. Cells were seeded at the same density in serum-free medium in the upper chamber, with 10% FBS-containing medium in the lower chamber as a chemoattractant. After 24 hours of incubation, non-migrated cells on the upper surface were removed, and migrated cells on the lower surface were fixed, stained, and counted.

2.10 Immunohistochemistry (IHC)

Tumor tissues were sectioned (4 µm thick), fixed, and paraffin-embedded. Sections were rehydrated with an alcohol gradient after being deparaffinized in xylene. 3% H_2O_2 was used to stop endogenous peroxidase activity for ten minutes. Using 0.01 mol/L sodium citrate buffer (ZSGB-BIO, Beijing, China, ZLI-9064) heated in a microwave, antigen retrieval was carried out. After blocking the sections for 20 minutes with 5% bovine serum albumin (Sigma-Aldrich, A1933), they were treated for an entire night at 4 °C with primary anti-Ki-67 (Abcam, ab15580, 1:500). Sections were incubated for 20 minutes at room temperature with a secondary antibody (ZSGB-BIO, PV-6000, 1:1000) the following day. Following washing, DAB substrate (ZSGB-BIO, ZLI-9018) was used for color development, and hematoxylin (ZSGB-BIO, ZLI-9609) was used for counterstaining. After being cleansed and dehydrated, stained slices were examined under a microscope.

2.11 Real-Time Quantitative PCR (qPCR)

TRIzol reagent (Thermo Fisher Scientific, 15596026) was used to extract total RNA from cells at the end of the 24-hour drug treatment period (i.e., 72 hours after transfection initiation for transfected groups, following the protocol in Section 2.1), and a reverse transcription kit (Thermo Fisher Scientific, K1622) was used to reverse-transcribe the RNA into cDNA. The SYBR Green technique was used for qPCR. A QuantStudio™ 5 Real-Time PCR System (Thermo Fisher Scientific) was used for amplification. The internal control was Actb. The $2^{-\Delta\Delta Ct}$ technique was used to calculate relative gene expression. The following were the primer sequences:

Human PIAS2:

F: 5′-AGCTGCATCTACCACCTCCA-3′, R: 5′-TGTAGCCGAGGTAGGCATTC-3′.

Human GPX4:

F: 5′-GAGGCAAGACCGAAGTAAACTAC-3′, R: 5′-CCGAACTGGTTACACGGGAA-3′.

Human β-actin:

F: 5′-CATGTACGTTGCTATCCAGGC-3′, R: 5′-CTCCTTAATGTCACGCACGAT-3′.

Mouse PIAS2:

F: 5′-GCTTGCAACACAGCAAGTCT-3′, R: 5′-TGTTGGCACTCAGGACACAG-3′.

Mouse GPX4:

F: 5′-GATTGGTCTGTCTGCACGTG-3′, R: 5′-GCCAGGCCTGTAGTATCCAA-3′.

Mouse β-actin:

F: 5′-CATTGCTGACAGGATGCAGA-3′, R: 5′-CTGCTGGAAGGTGGACAGTG-3′.

2.12 RNA Stability Assay

Actinomycin D (ActD, 5 μg/mL, MedChemExpress, HY-17559) was used to suppress transcription in HepG-2 and H22 cells that had been transfected with oe-NC or oe-PIAS2 constructs for 48 hours. Following ActD therapy, cells were collected at 0, 6, 12, and 24 hours. GPX4 mRNA levels were assessed by qPCR after total RNA was extracted. GPX4 mRNA expression at each time point was normalized to the corresponding 0-hour value within the same group (fold change relative to time 0) to evaluate mRNA decay kinetics. The complete timeline was: Day 0, cell seeding; Day 1, transfection; Day 3 (48 h post-transfection), ActD addition (0 h time point); 6, 12, and 24 hours after ActD, cell collection and RNA extraction. GPX4 mRNA abundance at each time point was normalized to the corresponding 0-h value within the same group, which was set to 1.0 (100%), and was reported as the relative remaining GPX4 mRNA level to evaluate mRNA decay over time.

2.13 Cycloheximide Chase Assay

HepG-2 and H22 cells were treated with cycloheximide (CHX, 100 μg/mL, MedChemExpress, HY-12320) to prevent protein synthesis after being transfected with oe-NC or oe-PIAS2 for 48 hours. At 0, 12, and 24 hours following CHX treatment, cells were collected. GPX4 protein levels were measured by Western blotting after total protein was extracted. Protein decay curves were generated by plotting the percentage of remaining GPX4 protein relative to time zero; however, formal curve fitting for half-life calculation was not performed. The complete timeline was: Day 0, cell seeding; Day 1, transfection; Day 3 (48 h post-transfection), CHX addition (0 h time point); 12 and 24 hours after CHX, cell collection and protein extraction. GPX4 protein abundance at 12 and 24 h was normalized to the corresponding 0-h value. The percentage of remaining GPX4 protein was plotted descriptively; formal kinetic curve fitting and half-life estimation were not performed.

2.14 Statistical Analysis

The information is displayed as mean ± standard deviation (SD). GraphPad Prism 8.0 (San Diego, California, USA) was used for statistical analysis. One-way analysis of variance (ANOVA) was used to examine differences between many groups, and LSD-t testing was used for pairwise comparisons. Statistical significance was defined as a p-value of less than 0.05.

3. Results

3.1 PIAS2 Overexpression Is Associated With Reduced Ferroptosis in HCC Cells

We initially looked at the expression of PIAS2 and GPX4 in HCC cells in order to look into the impact of PIAS2 on ferroptosis. HepG-2 and H22 cells treated with Era had substantially lower levels of PIAS2 mRNA and protein as well as GPX4 protein expression compared to the control group, according to qPCR and Western blotting ($p < 0.05$). On the other hand, PIAS2 and GPX4 expression levels were considerably higher in the Era+oe-PIAS2 group than in the Era+oe-NC group ($p < 0.05$). When compared to the Era group, co-treatment with Fer-1 did not substantially change PIAS2 expression ($p > 0.05$), but it did significantly restore GPX4 expression ($p < 0.05$, Fig. 1A,B). Further analysis of ferroptosis-related markers revealed that Era therapy significantly reduced GSH content and raised levels of lipid ROS, MDA, and Fe^{2+} in comparison to the control group ($p < 0.05$, Fig. 1C–F). Conversely, compared to the Era+oe-NC group, PIAS2 overexpression in the Era+oe-PIAS2 group significantly enhanced GSH content and decreased lipid ROS, MDA, and Fe^{2+} levels ($p < 0.05$, Fig. 1C–F). In contrast to the Era group, co-treatment with Fer-1 effectively reversed Era-induced ferroptosis, as seen by reduced lipid ROS and MDA levels, restored GSH content, and recovered Fe^{2+} levels ($p < 0.05$, Fig. 1C–F). These results indicate that PIAS2 inhibits Era-induced ferroptosis in HCC cells.

3.2 PIAS2 Overexpression Correlates With Reduced Ferroptosis and Is Accompanied by Increased Cell Viability, Migration, and Invasion Under Era-Treated Conditions

HepG-2 and H22 cell viability was considerably lower in the Era group than in the control group, according to the CCK-8 test findings ($p < 0.05$). Comparing the Era+oe-PIAS2 group to the Era+oe-NC group, PIAS2 overexpression considerably improved cell viability in the presence of Era ($p < 0.05$). In comparison to the Era group, co-treatment with Fer-1 also considerably improved cell viability ($p < 0.05$, Fig. 2A). Transwell assay results demonstrated that cells in the Era group exhibited reduced migratory and invasive capacities as compared with the control group ($p < 0.05$), whereas those in the Era+oe-PIAS2 group were considerably greater than those in the Era+oe-NC group under Era treatment ($p < 0.05$). Comparing these cells to the Era group, Fer-1 treatment considerably increased their ability to migrate and invade ($p < 0.05$, Fig. 2B). These results imply that under Era-induced ferroptotic conditions, PIAS2 overexpression is associated with changes in HCC cell motility, invasion, and cell viability within the context of Era challenge.

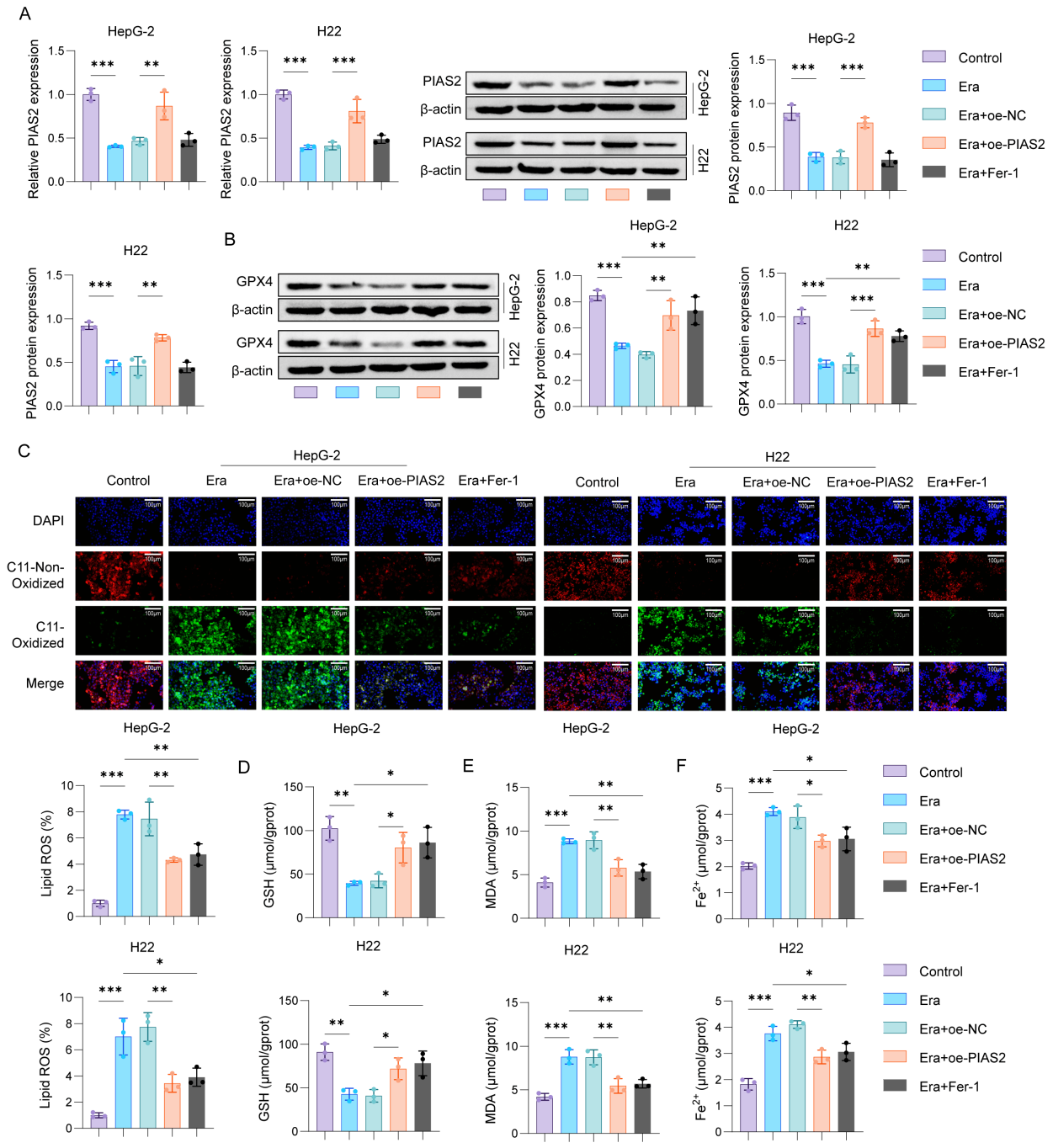

Fig. 1. PIAS2 overexpression is associated with reduced ferroptosis in HCC cells. (A) Western blotting and qPCR measurements of PIAS2 expression in HepG-2 and H22 cells. (B) GPX4 expression in HepG-2 and H22 cells was examined by Western blotting. (C–F) Measurement of lipid ROS (Scale bars: 100 μm), GSH, MDA, and Fe^{2+} levels in cells using appropriate commercial assay kits. n = 3, *p < 0.05, **p < 0.01, ***p < 0.001. PIAS2, Protein Inhibitor of Activated STAT 2; HCC, Hepatocellular Carcinoma; qPCR, Quantitative Real-Time Polymerase Chain Reaction; GPX4, Glutathione Peroxidase 4; ROS, Reactive Oxygen Species; GSH, Glutathione; MDA, Malondialdehyde; Era, Erastin. Unless otherwise indicated, n = 3 independent biological experiments performed using separately cultured and independently transfected cell batches.

3.3 PIAS2 Overexpression Is Associated With Regulation of GPX4 Levels and Enhanced SUMOylation

HepG-2 and H22 cells were subsequently treated with oe-PIAS2, sh-PIAS2, or comparable control constructs in order to explore the molecular association between PIAS2 and GPX4 regulation. Western blotting confirmed that overexpression of PIAS2 significantly upregulated both PIAS2 and GPX4 at the protein level compared to oe-NC group (p < 0.05, Fig. 3A). To assess SUMOylation, Flag-GPX4 was immunoprecipitated with anti-Flag and blot-

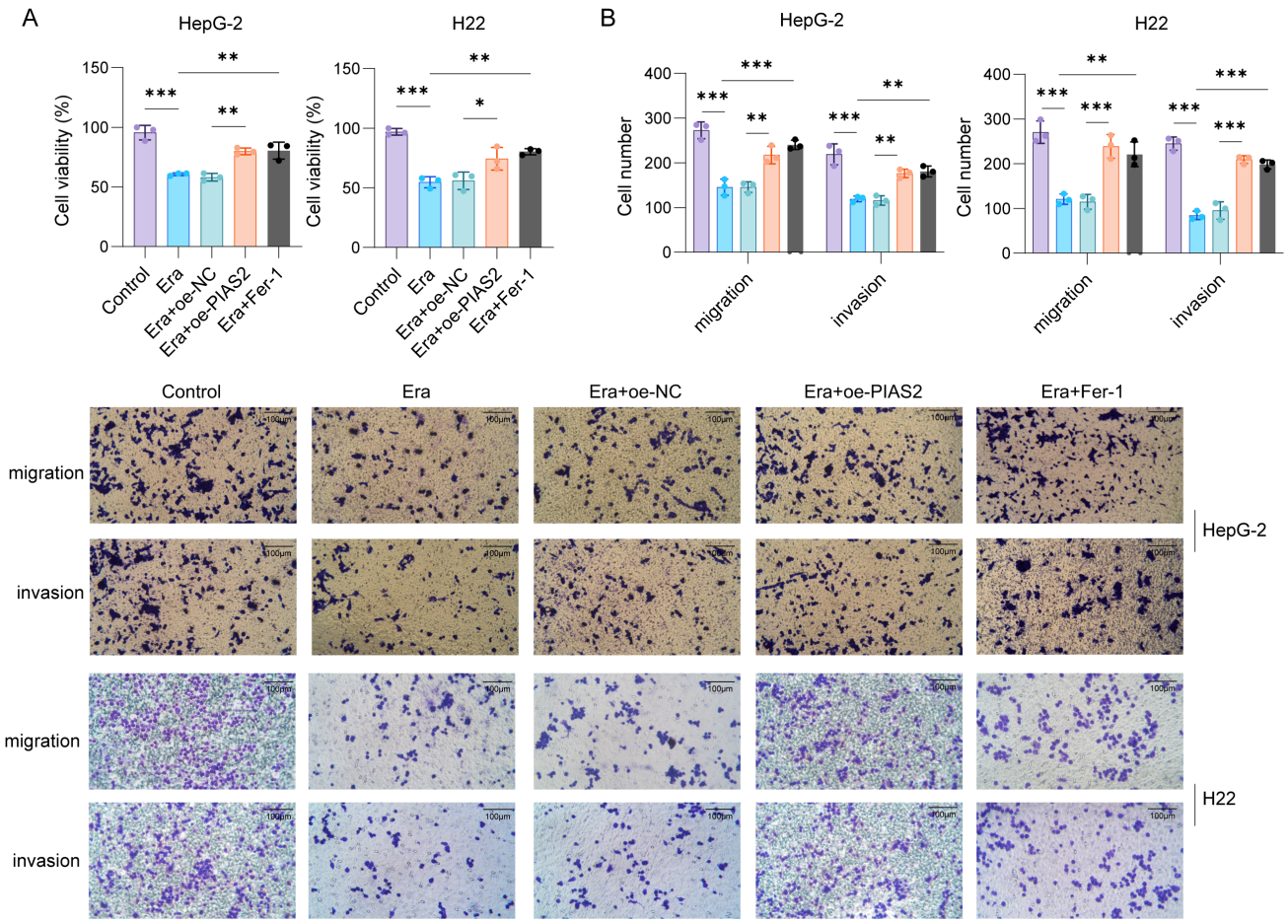

Fig. 2. PIAS2 overexpression correlates with reduced ferroptosis and is accompanied by increased cell viability, migration, and invasion under Era-treated conditions. (A) Cell viability study with CCK-8. (B) Transwell test for invasion and migration of cells (Scale bars: 100 µm). n = 3, *$p < 0.05$, **$p < 0.01$, ***$p < 0.001$. CCK-8, Cell Counting Kit-8. Unless otherwise indicated, n = 3 independent biological experiments performed using separately cultured and independently transfected cell batches.

ted for SUMO3. Whole cell lysates were also probed for Flag, SUMO3, PIAS2, and β-actin to confirm equal protein expression and successful immunoprecipitation. As shown in Fig. 3B, in both HepG-2 and H22 cells, the SUMO3-modified GPX4 band intensity appeared considerably higher in the oe-PIAS2 group than in the control treatment, while it appeared markedly lower in the sh-PIAS2 group than in the control group by visual inspection of the representative blots. Co-IP results confirmed co-immunoprecipitation of PIAS2 and GPX4 in both of these cell types, indicating that these two proteins are present in the same protein complex (Fig. 3C). To determine whether PIAS2 overexpression affects GPX4 mRNA stability, we first examined *GPX4* mRNA decay using actinomycin D chase assays. As shown in Fig. 3D, in both HepG-2 and H22 cells, the *GPX4* mRNA decay rate was considerably slower in the oe-PIAS2 group than in the oe-NC group at 6, 12, and 24 hours ($p < 0.05$, Fig. 3D). This indicates that PIAS2 overexpression is associated with reduced *GPX4* mRNA degradation, suggesting a regulatory effect at the post-transcriptional mRNA stability levels. Next, we used CHX chase experiments to investigate how PIAS2 overexpression affected the stability of the GPX4 protein. As shown in Fig. 3E, GPX4 protein levels gradually decreased over time following CHX treatment in both groups. However, at 12 and 24 hours, the rate of GPX4 protein decline in the oe-PIAS2 group was noticeably slower than that of the oe-NC group ($p < 0.05$, Fig. 3E). These results suggest that PIAS2 overexpression is associated with reduced GPX4 protein degradation, and this effect correlates with its physical association with GPX4 in cells and enhanced SUMOylation signals.

3.4 GPX4 Knockdown Is Associated With Attenuation of the Phenotypic Changes Observed With PIAS2 Overexpression in HCC Cells

GPX4 knockdown studies were then carried out to further explore whether GPX4 might be involved in the PIAS2-associated control of ferroptosis and HCC tumor growth in HCC cells. GPX4 expression was considerably lower in the Era+oe-NC+sh-NC group than in the oe-NC+sh-NC group for both examined cell lines, ac-

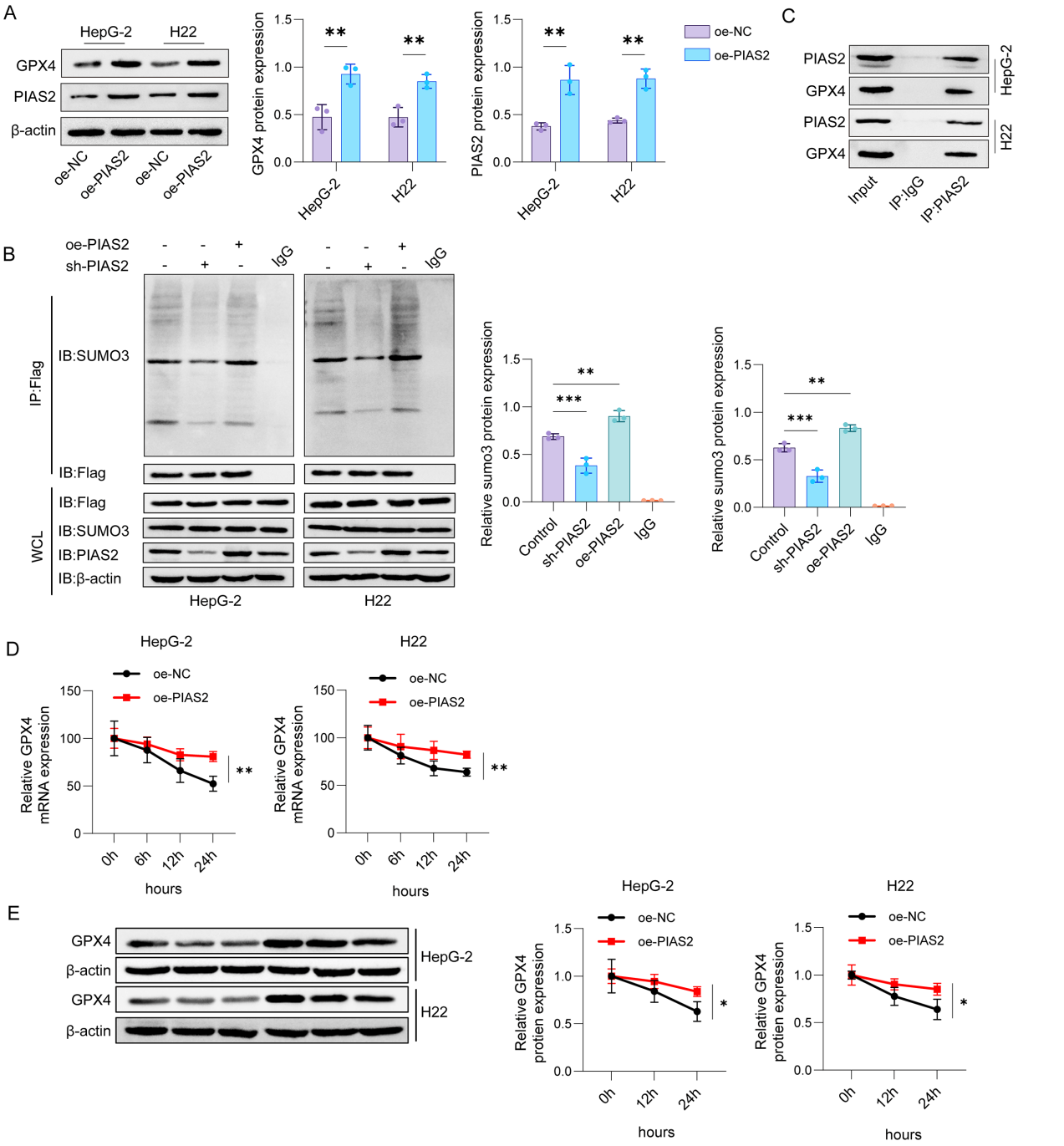

Fig. 3. PIAS2 overexpression is associated with regulation of GPX4 levels and enhanced SUMOylation. (A) Western blotting study of the levels of GPX4 and PIAS2 in HepG-2 and H22 cells. (B) Immunoprecipitation (IP)-based detection of GPX4 SUMOylation levels. (C) Co-IP assay analysis of PIAS2-GPX4 physical association. (D) Actinomycin D chase assay assessing *GPX4* mRNA stability. (E) CHX chase assay examining GPX4 protein stability. n = 3, *$p < 0.05$, **$p < 0.01$, ***$p < 0.001$. SUMO, Small Ubiquitin-like Modifier; Co-IP, Co-Immunoprecipitation; CHX, cycloheximide. Unless otherwise indicated, n = 3 independent biological experiments performed using separately cultured and independently transfected cell batches.

cording to Western blotting ($p < 0.05$). GPX4 expression was considerably higher in the PIAS2 overexpression group (Era+oe-PIAS2+sh-NC) than in the Era+oe-NC+sh-NC group ($p < 0.05$). However, knocking down GPX4 (Era+oe-PIAS2+sh-GPX4 group) markedly reversed this increase ($p < 0.05$, Fig. 4A). Ferroptosis marker analyses showed that, in comparison to the oe-NC+sh-NC group, the Era therapy (Era+oe-NC+sh-NC group) significantly raised lipid ROS, MDA, and Fe^{2+} levels while lowering GSH content ($p < 0.05$). PIAS2 overexpression ameliorated

these changes ($p < 0.05$), but subsequent GPX4 knockdown reversed the positive effects of PIAS2 overexpression on these phenotypes, resulting in higher lipid ROS, MDA, and Fe^{2+} levels along with a reduction in GSH content ($p < 0.05$, Fig. 4B–E). Cell viability, migration, and invasion were considerably lower in the Era+oe-NC+sh-NC group than in the oe-NC+sh-NC group, according to functional tests ($p < 0.05$). In comparison to the levels seen in the Era+oe-NC+sh-NC group, overexpressing PIAS2 increased the vitality, migratory, and invasive capabilities of these cells ($p < 0.05$), whereas GPX4 knockdown effectively attenuated this restoration ($p < 0.05$, Fig. 4F,G). These findings suggest that GPX4 knockdown attenuated the phenotypic changes associated with PIAS2 overexpression, indicating a possible involvement of GPX4 in the phenotypic effects linked to PIAS2 modulation in HCC cells.

3.5 PIAS2 Overexpression Is Associated With Increased Tumor Growth and Reduced Ferroptosis in Era-Treated Mice In Vivo

Tumor size, volume, and weight were significantly reduced in the Era group compared to the Control group in tumor-bearing mice ($p < 0.05$). Conversely, the Era+oe-PIAS2 group had substantially larger tumor size, volume, and weight than the Era+oe-NC group in Era-treated animals ($p < 0.05$, Fig. 5A). IHC analysis showed that Ki-67 staining intensity appeared substantially lower in the Era group than in the Control group by visual inspection, while it appeared higher in the Era+oe-PIAS2 group than in the Era+oe-NC group under Era treatment (Fig. 5B). According to Western blotting, tumors from the Era group had considerably lower levels of PIAS2 and GPX4 proteins than tumors from the control group ($p < 0.05$), but tumors from the Era+oe-PIAS2 group had significantly greater levels than those from the Era+oe-NC group in the presence of Era ($p < 0.05$, Fig. 5C). Analyses of intratumoral GSH, MDA, and Fe^{2+} levels further revealed that the Era group had decreased GSH content and considerably higher MDA and Fe^{2+} levels than the Control group ($p < 0.05$). In contrast, when compared to the Era+oe-NC group, the Era+oe-PIAS2 group showed considerably reduced MDA and Fe^{2+} levels together with greater GSH content under Era treatment ($p < 0.05$, Fig. 5D–F). These *in vivo* results confirm that PIAS2 overexpression is associated with reduced ferroptotic activity while correlating with increased HCC tumor growth in Era-treated mice.

4. Discussion

HCC remains a highly prevalent form of cancer throughout the globe, and is characterized by strong invasiveness and poor prognostic outcomes. The development of tailored therapy approaches appropriate for clinical application may be facilitated by research aimed at identifying the primary molecular pathways driving its malignant growth. Ferroptosis is a unique type of controlled cell death that is crucial to the formation, initiation, and response to therapy of tumors. Lipid peroxide buildup, iron-dependent oxidative damage, and disruption of the antioxidant system are all components of ferroptotic cell death. GPX4 is a fundamental antioxidant enzyme that can prevent ferroptosis by removing lipid peroxides [19]. By mediating the SUMOylation of target proteins, PIAS2, a significant SUMO E3 ligase, influences a number of biological processes, such as tumor cell growth and apoptosis [20]. According to the findings of this study, under the Era treatment conditions, PIAS2 overexpression is associated with HCC cell viability, migration, invasion, and *in vivo* tumor development in a manner that correlates with enhanced GPX4 SUMOylation and reduced ferroptosis in HCC cells. These results point to this route as a novel target for treatment of HCC.

As ferroptosis is a form of programmed cell death controlled by the GPX4-mediated lipid antioxidant system, the dysregulation of the regulatory pathway is closely linked to the progression of HCC and other malignancies. This has spurred growing interest in targeting the ferroptosis pathway to guide HCC treatment [21,22]. Era is a well-known ferroptosis inducer that starts this type of cell death by lowering GSH levels, decreasing GPX4 activity, and blocking system Xc-activity [23]. In this study, we first used Era treatment to establish a model of ferroptotic induction in HCC cells. In these experiments, Era treatment dramatically reduced the expression of GPX4 and PIAS2 in HepG-2 and H22 cells, accompanied by characteristic changes in ferroptosis markers. Overexpression of PIAS2 effectively reversed these changes, upregulating GPX4 expression and inhibiting Era-induced ferroptosis. These findings are consistent with a ferroptosis-suppressive role of PIAS2 in HCC cells, suggesting that PIAS2 may be involved in the regulation of ferroptosis and tumor cell survival. In line with our findings, Wu et al. [24] reported that PIAS2 binds to and enhances the activity of the Zinc Finger Homeobox 3 (ZFHX3) transcription factor, thereby accelerating cancer cell proliferation. The processes of tumor development and metastasis depend on the tumor cells' capacity to multiply, move, and infect neighboring tissues. The connection between ferroptosis and these malignant behaviors has become a focus of intensive research interest [25]. Experimental evidence has confirmed that inhibiting ferroptosis enhances malignant phenotypes, whereas ferroptotic induction suppresses tumor progression [26,27,28]. Our results support these findings, demonstrating that Era-induced ferroptosis significantly reduces HCC cell viability and inhibits both migratory and invasive activity. PIAS2 overexpression attenuates ferroptosis under Era treatment, thereby markedly reversing the suppressive effects of Era, restoring cell viability, and enhancing migratory and invasive activity in the context of Era challenge. It should be noted that Transwell migration and invasion results may be partially influenced by differences in cell viability, as reduced viability

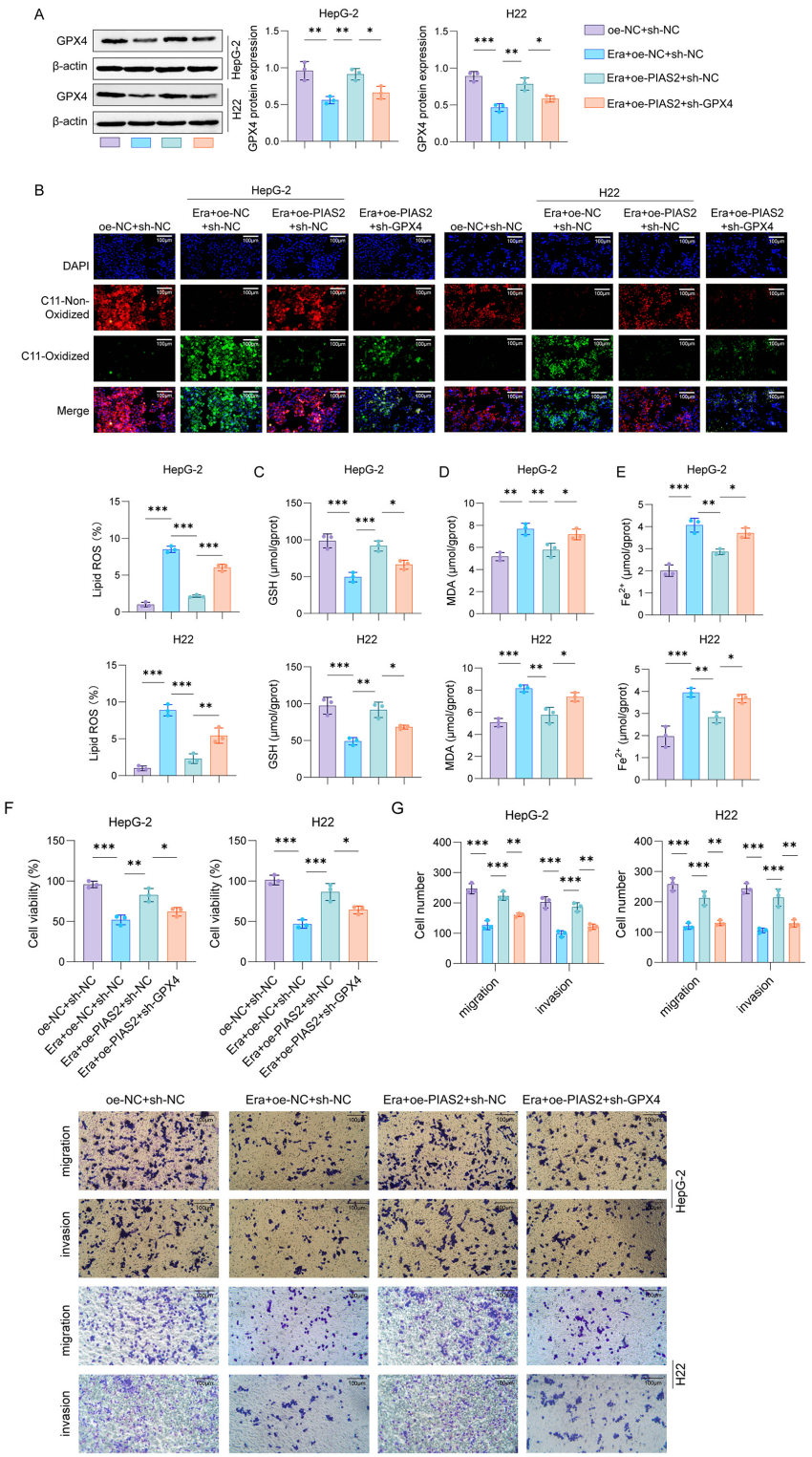

Fig. 4. GPX4 knockdown is associated with attenuation of the phenotypic changes observed with PIAS2 overexpression in HCC cells. (A) GPX4 expression in HepG-2 and H22 cells exposed to the specified conditions was examined using Western blotting. (B–E) Lipid ROS (Scale bars: 100 μm), GSH, MDA, and Fe^{2+} levels in cells from the indicated treatment groups. (F) Investigation of cell viability using the CCK-8 test. (G) Analysis of cell invasion and migration using transwell assays (Scale bars: 100 μm). n = 3, *$p < 0.05$, **$p < 0.01$, ***$p < 0.001$. Unless otherwise indicated, n = 3 independent biological experiments performed using separately cultured and independently transfected cell batches.

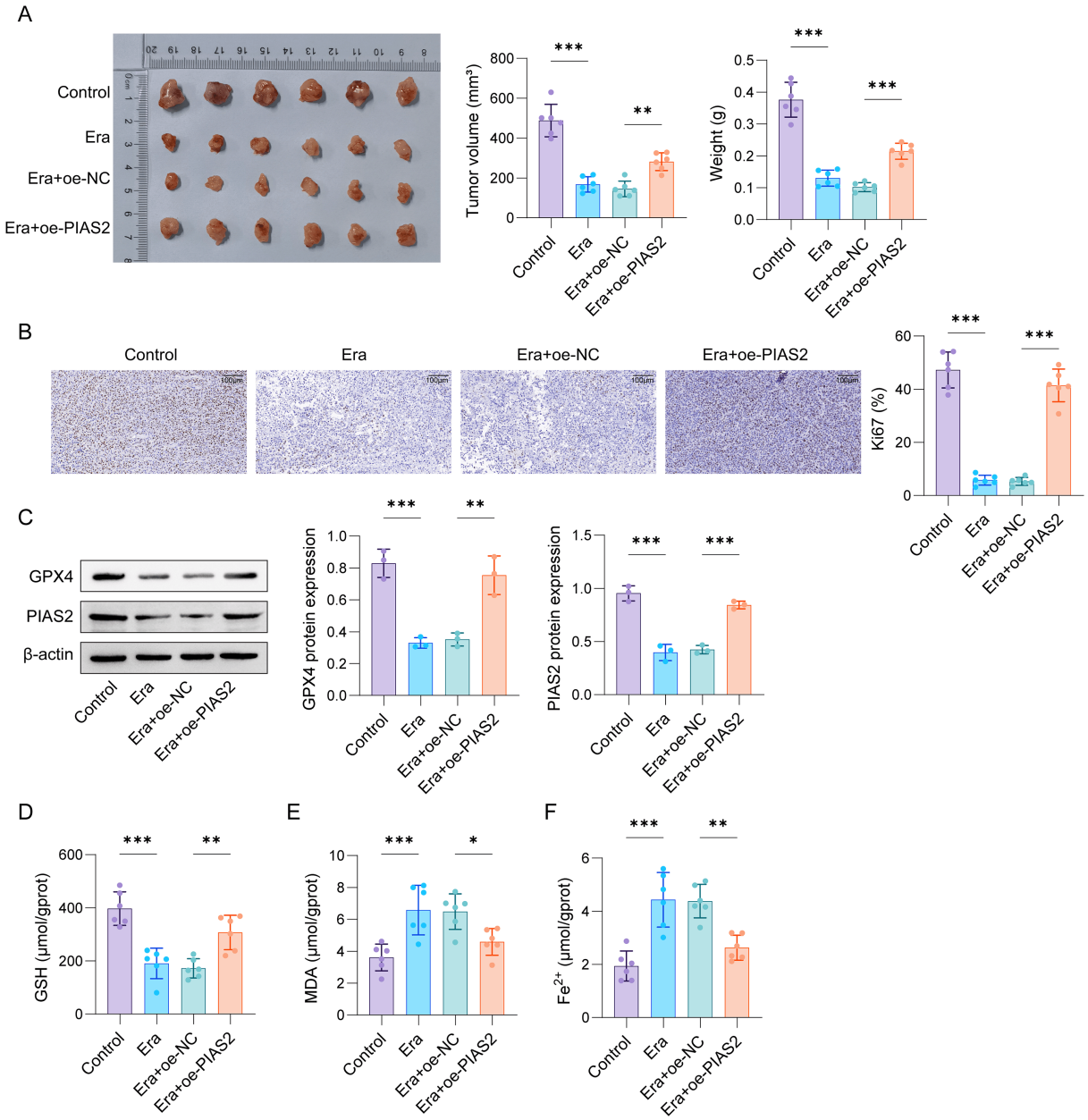

Fig. 5. PIAS2 overexpression is associated with increased tumor growth and reduced ferroptosis in Era-treated mice *in vivo*. (A) Tumor appearance, volume, and weight in mice from the indicated groups. (B) Ki-67 expression in tumor tissues as determined by immunohistochemistry (Scale bars: 100 μm). (C) Western blotting study of tumor tissue expression of GPX4 and PIAS2, n = 3. (D–F) GSH, MDA, and Fe^{2+} levels as measured in tumor tissue samples. n = 6, *$p < 0.05$, **$p < 0.01$, ***$p < 0.001$. For Western blotting in panel C, n = 3 independent tumor samples per group. For tumor growth and biochemical measurements in panels A and D–F, n = 6 mice per group. Each mouse was treated as one biological replicate.

could indirectly affect the number of cells available to migrate or invade. However, the consistency of effects across multiple assays supports a ferroptosis-associated contribution to these phenotypic changes. We further performed validation experiments using the specific ferroptosis inhibitor Fer-1, revealing that co-treatment with Fer-1 effectively reversed Era-induced changes in ferroptosis-related markers, including decreased lipid ROS, MDA, and Fe^{2+} levels, while also restoring GSH content and rescuing Era-associated changes in cell viability, migration, and invasion. Notably, Fer-1 treatment did not significantly affect PIAS2 expression, but it effectively restored GPX4 protein levels, indicating an association between GPX4 restoration and the reversal of ferroptotic changes. These findings are consistent with the interpretation that the phenotypic changes associated with PIAS2 overexpression under Era-induced conditions are closely linked to modulation of the ferroptosis pathway, although the possibility of con-

tributions from other pathways cannot be excluded. Consistent with this, studies in HepG-2 and Huh7 cells have previously demonstrated that Era significantly reduces viability and migratory activity, while N-Myc Downstream Regulated Gene 1 (NDRG1) knockdown further amplifies these effects, accompanied by elevated Fe^{2+}, ROS, and lipid-ROS levels and morphological changes consistent with pronounced ferroptotic induction [29]. Furthermore, *in vivo* tumor investigations in Era-treated animals showed that PIAS2 overexpression markedly increased tumor development, tumor volume and weight, and Ki-67 expression in tumor tissues from Era-treated animals, which is consistent with our *in vitro* findings. These consistent *in vitro* and *in vivo* findings obtained under ferroptotic induction conditions suggest that PIAS2 overexpression is associated with phenotypic changes that correlate with reduced ferroptosis in HCC, highlighting a potential association that may be relevant to HCC development under ferroptotic stress. However, it should be emphasized that the *in vivo* experiments were limited to the detection of PIAS2, GPX4, Ki-67, and redox markers, and did not assess GPX4 SUMO3 modification, the PIAS2–GPX4 complex, or perform genetic reversal experiments in tumor tissues. Future studies incorporating *in vivo* SUMOylation detection, co-immunoprecipitation from tumor tissues, and genetic rescue experiments will be required to confirm this mechanistic axis in the physiological context.

PIAS family proteins are important SUMO-conjugating enzymes that regulate target protein stability, localization, and function via SUMOylation [30]. SUMOylation of many tumor-associated proteins has been linked to PIAS2 [31]. The protein level stability of GPX4 is essential for it to effectively regulate ferroptosis through its core antioxidant functions [32], and post-translational SUMOylation can modulate GPX4 stability and activity [33]. Here, the association between PIAS2 and GPX4 was explored in greater detail, revealing that PIAS2 overexpression significantly upregulated GPX4 protein levels and was associated with enhanced GPX4 SUMO3 modification in HCC cells. Co-IP experiments confirmed co-immunoprecipitation between PIAS2 and GPX4, indicating that these two proteins exist in the same complex in cells, which is consistent with the notion that PIAS2 may influence GPX4 by associating with it and correlating with its SUMOylation. Furthermore, the actinomycin D chase experiment revealed that PIAS2 overexpression is associated with a slower decay rate of GPX4 mRNA, suggesting a potential effect at the post-transcriptional level. By contrast, the cycloheximide chase experiment demonstrated that PIAS2 overexpression correlates with a slower decline in GPX4 protein levels, which may be mechanistically linked to SUMOylation-mediated enhancement of protein stability. We then conducted rescue studies to shed light on GPX4's function in the PIAS2-mediated control of ferroptosis and the malignant development of HCC under Era challenge. This method demonstrated that GPX4 knockdown effectively reversed the elevation of GPX4 seen in response to PIAS2 overexpression and attenuated PIAS2's inhibitory influence on ferroptosis, resulting in elevated levels of lipid ROS, MDA, and Fe^{2+} along with a decrease in GSH content. Moreover, the increases in cell viability, migratory, and invasive activities associated with PIAS2 overexpression under Era-treated conditions were successfully attenuated by GPX4 knockdown. These rescue experiments suggest that PIAS2 overexpression is associated with enhanced GPX4 protein levels and SUMOylation signals, and that GPX4 knockdown attenuates these effects, raising the possibility that GPX4 may contribute to the phenotypic changes associated with PIAS2 modulation under erastin-induced ferroptotic stress. In further support of a potential link between SUMOylation regulation and GPX4, Wang et al. [34] discovered that via de-SUMOylating β-catenin, Sentrin/SUMO-Specific Protease 5 (SENP5) increases GPX4 expression, preventing ferroptosis and accelerating the development of endometrial cancer.

5. Limitations

First, although SUMO3 was selected as the focus of the current study based on our preliminary screening, we did not examine other SUMO isoforms, such as SUMO1 or SUMO2. Given that PIAS2 also reportedly plays a role in influencing these modifications, we cannot rule out the possibility that PIAS2 may additionally modulate GPX4 function through SUMO1 or SUMO2 conjugation. Future studies focused on the systematic evaluation of all SUMO paralogs will be necessary to fully elucidate the spectrum of PIAS2-mediated GPX4 SUMOylation. Second, due to time constraints, we were unable to perform comprehensive PIAS2 knockdown/knockout experiments to further verify its regulatory effects on ferroptosis and its association with GPX4 SUMOylation. We plan to conduct experiments in future investigations through the use of CRISPR/Cas9-mediated knockout or siRNA-mediated knockdown approaches. Third, while all of our results point to a regulatory function for PIAS2 in the SUMOylation and expression of GPX4, they do not provide definitive proof that PIAS2 acts as a direct SUMO E3 ligase for GPX4. To confirm this direct regulatory relationship, *in vitro* SUMOylation assays would need to be conducted using purified proteins to demonstrate direct enzymatic activity. Fourth, while our rescue experiments demonstrate that GPX4 knockdown attenuates several phenotypic changes associated with PIAS2 overexpression, they do not establish GPX4 as the sole or definitive downstream mediator of PIAS2, nor do they prove a direct regulatory relationship. Future studies, such as proteomic screening or rescue experiments with SUMOylation-deficient GPX4 mutants, will be essential to determine the specificity of the PIAS2-GPX4 axis. Fifth, due to the limited availability

of well-annotated clinical specimens, we were unable to validate the clinical relevance of the PIAS2-GPX4 axis in HCC patient samples. Its translational importance has to be confirmed by additional research using separate cohorts. These limitations may partially constrain the direct translational implications of our current findings, but they also open promising avenues for future investigations, including site-directed mutagenesis studies, approaches employing immunocompetent mouse models, and retrospective or prospective clinical analyses.

6. Conclusion

In summary, this work shows that PIAS2 and GPX4 co-immunoprecipitate in HCC cells, and PIAS2 overexpression is associated with enhanced SUMOylation signals and stabilization as well as upregulation of GPX4 protein levels. Under erastin-induced ferroptotic conditions, this correlates with increased resistance of HCC cells to ferroptosis, which is accompanied by restoration of tumor cell invasion, cell viability, and *in vivo* tumor development in the context of Era challenge. Furthermore, GPX4 knockdown attenuated the phenotypes observed under PIAS2 overexpression, suggesting possible involvement of GPX4. These discoveries provide fresh perspectives to guide HCC treatment while also extending our knowledge of SUMOylation's function in tumor metabolism and cell death. Targeting PIAS2 or its association with GPX4 SUMOylation may represent an effective approach to disrupting ferroptotic defenses in tumor cells, rendering them more sensitive to existing treatments.

Abbreviations

PIAS2, Protein Inhibitor of Activated STAT 2; GPX4, Glutathione Peroxidase 4; SUMO, Small Ubiquitin-like Modifier; HCC, Hepatocellular Carcinoma; Era, Erastin; Co-IP, Co-Immunoprecipitation; ROS, Reactive Oxygen Species; MDA, Malondialdehyde; GSH, Glutathione; qPCR, Quantitative Real-Time Polymerase Chain Reaction; IHC, Immunohistochemistry; FBS, Fetal Bovine Serum; AAV, Adeno-Associated Virus; CCK-8, Cell Counting Kit-8; ZFHX3, Zinc Finger Homeobox 3; NDRG1, N-Myc Downstream Regulated Gene 1; MK2, MAPK-Activated Protein Kinase 2; SENP5, Sentrin/SUMO-Specific Protease 5.

Availability of Data and Materials

The datasets used or analyzed during the current study are available from the corresponding author on reasonable request.

Author Contributions

XC, JY, and MY guaranteed the integrity of the entire study. XC and LF designed the study and literature research. JY and XD defined the intellectual content. XC, JY, and MY performed experiment. LF, ZF, and MY collected the data. XD, ZF and LF analyzed the data. XC and JY drafted the primary manuscript and produced the figures. All authors contributed to editorial changes in the manuscript. All authors read and approved the final manuscript. All authors have participated sufficiently in the work and agreed to be accountable for all aspects of the work.

Ethics Approval and Consent to Participate

All animal procedures were conducted in accordance with international ethical guidelines for laboratory animal care. Animal study was approved by the Institutional Animal Care and Use Committee of Zhejiang Provincial Laboratory Animal Center (Approval No.: ZJCLA-IACUC-20011376). The study was carried out in accordance with the ARRIVE guidelines.

Acknowledgment

Not applicable.

Funding

This work was supported by the Zhejiang Provincial Natural Science Foundation of China (grant number: LY22H160044).

Conflicts of Interest

The authors declare no conflicts of interest.

Supplementary Material

Supplementary material associated with this article can be found, in the online version, at https://doi.org/10.31083/FBL53367.

References

[1] Zhan Z, Chen B, Huang R, Lin W, Lan S, Yao X, et al. Long-term trends and future projections of liver cancer burden in China from 1990 to 2030. Scientific Reports. 2025; 15: 13120. https://doi.org/10.1038/s41598-025-96615-1

[2] Carrera E, Abarca J, Acuña J, Almagro M, Armas D, Borja C, et al. Survival Outcomes in Hepatocellular Carcinoma: Experience from a Multidisciplinary Committee in Ecuador. Life (Basel, Switzerland). 2025; 15: 1565. https://doi.org/10.3390/life15101565

[3] Ru Q, Li Y, Chen L, Wu Y, Min J, Wang F. Iron homeostasis and ferroptosis in human diseases: mechanisms and therapeutic prospects. Signal Transduction and Targeted Therapy. 2024; 9: 271. https://doi.org/10.1038/s41392-024-01969-z

[4] Zhao L, Xu Z, Ren L, Zheng S, Gao J, Che H, et al. Investigating the relationship between peripheral blood transferrin receptor protein and tumor cell ferroptosis, invasion, and metastasis in bladder cancer. Scientific Reports. 2025; 15: 32197. https://doi.org/10.1038/s41598-025-12187-0

[5] Wang T, Gong M, Cao Y, Zhao C, Lu Y, Zhou Y, et al. Persistent ferroptosis promotes cervical squamous intraepithelial lesion development and oncogenesis by regulating KRAS expression in patients with high risk-HPV infection. Cell Death Discovery. 2022; 8: 201. https://doi.org/10.1038/s41420-022-01013-5

[6] Luo L, Wang H, Tian W, Zeng J, Huang Y, Luo H. Targeting ferroptosis for cancer therapy: iron metabolism and anticancer immunity. American Journal of Cancer Research. 2021; 11: 5508–5525.
[7] Zeng K, Huang N, Liu N, Deng X, Mu Y, Zhang X, et al. LACTB suppresses liver cancer progression through regulation of ferroptosis. Redox Biology. 2024; 75: 103270. https://doi.org/10.1016/j.redox.2024.103270
[8] Tang J, Long G, Xiao L, Zhou L. USP8 positively regulates hepatocellular carcinoma tumorigenesis and confers ferroptosis resistance through β-catenin stabilization. Cell Death & Disease. 2023; 14: 360. https://doi.org/10.1038/s41419-023-05747-7
[9] Su Z, Ding Y, Xue J, Sun J, Ji C. Identifying SUMOylation-related genes in liver fibrosis with bioinformatics and experimental models for diagnostic insights. Scientific Reports. 2025; 15: 39783. https://doi.org/10.1038/s41598-025-23516-8
[10] Wang P, Qiu J, Fang Y, Li S, Liu K, Cao Y, et al. SENP3 inhibition suppresses hepatocellular carcinoma progression and improves the efficacy of anti-PD-1 immunotherapy. Cell Death and Differentiation. 2025; 32: 959–972. https://doi.org/10.1038/s41418-024-01437-9
[11] Zhang Q, Zhang J, Lan T, He J, Lei B, Wang H, et al. Integrative analysis revealed a correlation of PIAS family genes expression with prognosis, immunomodulation and chemotherapy. European Journal of Medical Research. 2024; 29: 195. https://doi.org/10.1186/s40001-024-01795-7
[12] Lu S, Liu Z, Qi M, Wang Y, Chang L, Bai X, et al. Ferroptosis and its role in osteoarthritis: mechanisms, biomarkers, and therapeutic perspectives. Frontiers in Cell and Developmental Biology. 2024; 12: 1510390. https://doi.org/10.3389/fcell.2024.1510390
[13] Zhou L, Lian G, Zhou T, Cai Z, Yang S, Li W, et al. Palmitoylation of GPX4 via the targetable ZDHHC8 determines ferroptosis sensitivity and antitumor immunity. Nature Cancer. 2025; 6: 768–785. https://doi.org/10.1038/s43018-025-00937-y
[14] Cai H, Yang J, Luo F, Gan W, Li Y, Zhang L, et al. TP63 as a modulator of ferroptosis in TP53 mutations glioblastoma. Cell Death & Disease. 2025; 16: 614. https://doi.org/10.1038/s41419-025-07938-w
[15] Sheng Z, Zhu J, Deng YN, Gao S, Liang S. SUMOylation modification-mediated cell death. Open Biology. 2021; 11: 210050. https://doi.org/10.1098/rsob.210050
[16] Jiang H, Li Q, Yang X, Jia L, Cheng H, Wang J, et al. Bone marrow stromal cells protect myeloma cells from ferroptosis through GPX4 deSUMOylation. Cancer Letters. 2025; 611: 217388. https://doi.org/10.1016/j.canlet.2024.217388
[17] Qi W, Li Z, Xia L, Dai J, Zhang Q, Wu C, et al. LncRNA GABPB1-AS1 and GABPB1 regulate oxidative stress during erastin-induced ferroptosis in HepG2 hepatocellular carcinoma cells. Scientific Reports. 2019; 9: 16185. https://doi.org/10.1038/s41598-019-52837-8
[18] Yang Y, Liu T, Hu C, Xia H, Liu W, Chen J, et al. Ferroptosis inducer erastin downregulates androgen receptor and its splice variants in castration-resistant prostate cancer. Oncology Reports. 2021; 45: 25. https://doi.org/10.3892/or.2021.7976
[19] Hu Y, Li Z, Li M, Wu X, Zhang S, Tang M, et al. Targeting PRDX6-dependent localization and function of GPX4 enhances ferroptosis-mediated tumor suppression. Molecular Cell. 2025; 85: 4602–4620.e9. https://doi.org/10.1016/j.molcel.2025.11.023
[20] Li C, Boutet A, Pascariu CM, Nelson T, Courcelles M, Wu Z, et al. SUMO Proteomics Analyses Identify Protein Inhibitor of Activated STAT-Mediated Regulatory Networks Involved in Cell Cycle and Cell Proliferation. Journal of Proteome Research. 2023; 22: 812–825. https://doi.org/10.1021/acs.jproteome.2c00557
[21] Yang L, Guan Y, Liu Z. Role of ferroptosis and its non-coding RNA regulation in hepatocellular carcinoma. Frontiers in Pharmacology. 2023; 14: 1177405. https://doi.org/10.3389/fphar.2023.1177405
[22] Liu Y, Zhao J, Cong W, Liu T, Sha K. Alpinetin pretreatment prevents lipopolysaccharide/D-galactosamine-induced acute liver injury in mice by inhibiting ferroptosis via the Nrf2/SLC7A11/GPX4 pathway. Scientific Reports. 2025; 15: 40065. https://doi.org/10.1038/s41598-025-26588-8
[23] Liu J, Dong R, Yuan B, Xie Y, Feng Z, Zhou S, et al. Immune cells dying from ferroptosis: mechanisms and therapeutic opportunities. Cell Death & Disease. 2025; 16: 878. https://doi.org/10.1038/s41419-025-08204-9
[24] Wu R, Fang J, Liu M, A J, Liu J, Chen W, et al. SUMOylation of the transcription factor ZFHX3 at Lys-2806 requires SAE1, UBC9, and PIAS2 and enhances its stability and function in cell proliferation. The Journal of Biological Chemistry. 2020; 295: 6741–6753. https://doi.org/10.1074/jbc.RA119.012338
[25] Jiang Z, Zhou J, Deng J, Li L, Wang R, Han Y, et al. Emerging roles of ferroptosis-related miRNAs in tumor metastasis. Cell Death Discovery. 2023; 9: 193. https://doi.org/10.1038/s41420-023-01486-y
[26] Sakai AH, Pereira ÉR, Santos AGPD, Quadreli DH, Lima LVAD, Ribeiro DL, et al. miR-25-3p Modulates Tumor Aggressiveness and Ferroptosis Escape in T24 Bladder Cancer Cells In Vitro. Pharmaceuticals (Basel, Switzerland). 2025; 18: 1382. https://doi.org/10.3390/ph18091382
[27] Yuan S, Xi S, Weng H, Guo MM, Zhang JH, Yu ZP, et al. YTHDC1 as a tumor progression suppressor through modulating FSP1-dependent ferroptosis suppression in lung cancer. Cell Death and Differentiation. 2023; 30: 2477–2490. https://doi.org/10.1038/s41418-023-01234-w
[28] Zhong Y, Wu L, Peng Z, Mao W, Wang T, Wu B, et al. LONP1 Promotes Hepatocarcinogenesis by Degrading ACO2 to Alleviate Ferroptosis. Frontiers in Bioscience (Landmark Edition). 2025; 30: 41226. https://doi.org/10.31083/FBL41226
[29] Li L, Wu T, Gong G, Li B, Feng J, Xu L, et al. NDRG1 alleviates Erastin-induced ferroptosis of hepatocellular carcinoma. BMC Cancer. 2025; 25: 522. https://doi.org/10.1186/s12885-025-13954-y
[30] Li C, McManus FP, Plutoni C, Pascariu CM, Nelson T, Alberici Delsin LE, et al. Quantitative SUMO proteomics identifies PIAS1 substrates involved in cell migration and motility. Nature Communications. 2020; 11: 834. https://doi.org/10.1038/s41467-020-14581-w
[31] Lara-Ureña N, Jafari V, García-Domínguez M. Cancer-Associated Dysregulation of Sumo Regulators: Proteases and Ligases. International Journal of Molecular Sciences. 2022; 23: 8012. https://doi.org/10.3390/ijms23148012
[32] Huang B, Wang H, Liu S, Hao M, Luo D, Zhou Y, et al. Palmitoylation-dependent regulation of GPX4 suppresses ferroptosis. Nature Communications. 2025; 16: 867. https://doi.org/10.1038/s41467-025-56344-5
[33] Cui C, Yang F, Li Q. Post-Translational Modification of GPX4 is a Promising Target for Treating Ferroptosis-Related Diseases. Frontiers in Molecular Biosciences. 2022; 9: 901565. https://doi.org/10.3389/fmolb.2022.901565
[34] Wang Z, Zhang Y, Zhang Y, Deng Q, Xi Y, He W, et al. SENP5 promotes endometrial cancer cell growth by regulating β-catenin deSUMOylation to enhance GPX4-resistance to ferroptosis. European Journal of Medical Research. 2025; 30: 411. https://doi.org/10.1186/s40001-025-02662-9